DANMARKS OG GRØNLANDS GEOLOGISKE UNDERSØGELSE RAPPORT 1999/18

EFP-98 Rock physics of Chalk: Analysis of acoustic log data from the well SA-1, South Arne field

ENS J.nr. 1313/98-007

Lars Gommesen & Peter Japsen

GEOLOGICAL SURVEY OF DENMARK AND GREENLAND
MINISTRY OF ENVIRONMENT AND ENERGY

G E U S

DANMARKS OG GRØNLANDS GEOLOGISKE UNDERSØGELSE RAPPORT 1999/18

EFP-98 Rock physics of Chalk: Analysis of acoustic log data from the well SA-1, South Arne field

ENS J.nr. 1313/98-007

Lars Gommesen & Peter Japsen

Released 01.05.2005

GEOLOGICAL SURVEY OF DENMARK AND GREENLAND
MINISTRY OF ENVIRONMENT AND ENERGY

G E U S

Summary

The acoustic and elastic properties of the Tor Formation in well SA-1 have been studied with respect to the influence of effective stress, porosity, pore fluid. The acoustic properties are found to be influenced by pore fluid and porosity. The V_p-V_s ratio for the Tor Formation clearly reflects whether the pore fluid is oil or brine, and porosity is found to correlate with both V_p and V_s, impedance and bulk modulus. Fluid substitution has been performed, and linear average trends have been established between porosity and V_p, V_s and impedance for the Tor Formation saturated with brine. The acoustic properties are unaffected by variations in effective stress over the studied interval.

Introduction

This report is part of the EFP-98 project Rock Physics of Chalk, and presents the results of an analysis of the acoustic log data measured in well SA-1. The report focuses on the acoustic and elastic properties of the Tor Formation, but data from the Ekofisk formation are included for comparison.

The study of the acoustic and the elastic properties of the Tor and Ekofisk formations is primarily based on the acoustic response recorded by the DSI log (Dipole Sonic Imager). Whereas the acoustic properties are studied directly from the measured compressional and shear waves velocities, the elastic properties are based on the dynamic, elastic moduli. These moduli are calculated from acoustic (DSI) and density log data.

In carbonate rock the compressional wave and shear wave velocities are mainly controlled by porosity. Several other intrinsic and extrinsic parameters influence on the acoustic properties of the rock. The first group of parameters includes fluid type, texture, and lithology, whereas the latter group includes effective stress and wave frequency. The influence of porosity, pore fluid, and effective stress are analysed with respect to rock physics theory and by the use of the PetroTools software.

Formations & zones

The studied interval of well SA-1 is from top chalk to base Tor. According to the composite well log *SA-1 Flank pilot* (Amerada Hess A/S, 1998) the Tor and Ekofisk formations are represented respectively by the zones TA - TD and EF – EG (Table 1).

Formation	*Zones*	*MDRT [m]*	*TVDSS [m]*
Ekofisk	EFii, EFi, EGii, EGi/LAG	3316.5; 3360.5	-2781.4; -2810.8
Tor	TAiii, TAii, TAi, TB/TC, TD	3360.5; 3480.0	-2810.8; -2889.7

Table 1. Stratigraphy of the logged chalk interval of well SA-1 (Amerada Hess A/S). In Ekofisk formation EFii is the uppermost and in Tor formation TAii is the uppermost.

Logs and control parameters

Several logs have been used in this study (Table 2). All logs are correlated by depth and given by MDRT, TVDRT, TVDSS (see Parameters for description of logs). All data of the mentioned logs are included in the analysis and no data has been edited or deleted.

Log name	*Origin*
VCA	1-VSHmin, see text below.
VSHmin	GEUS.
DTCO	Amerada Hess (Schlumberger).
DTSH	Amerada Hess (Schlumberger).
Effective stress	See Effective stress paragraph.
PHI_e	GEUS.
RHO_z	Amerada Hess (Schlumberger).
SONIC	Amerada Hess (Schlumberger).
So	1-Sw, see text below.
Sw	GEUS.
Temp	Amerada Hess (Schlumberger).

Table 2. Logs used as input for the acoustic study.

The mineralogical composition of the reservoir rock is simplified to be composed only by chalk and clay. Thus one minus clay content is calculated to be equal to chalk content.
Also the fluid composition of the reservoir fluid is simplified to be composed only by brine and oil, therefore one minus water saturation is calculated to be equal to the oil saturation.

Synthetic density and velocity logs for solids and fluids are generated in PetroTools on basis of the logs in Table 2 and control parameters defined in Petrotools (Table 3). The velocity logs representing the solid phase ($V_{p,solid}$ and $V_{s,solid}$) are calculated on basis of the control parameters of calcite and clay (shear and bulk modulus) and the volume fractions of these two minerals. The $V_{p,solid}$ and $V_{s,solid}$ are hereby estimated independent from porosity. Petrotools generate the effective moduli of a multiphase (here a two-phase) composite by the use of the Voigt-Reuss-Hill average (Equation 1).

Equation 1

$$M_{Voigt\,ReussHill} = \frac{M_{Voigt} + M_{Reuss}}{2},$$

Equation 2

$$M_{Voigt} = \sum_{i=1}^{N} f_i M_i,$$

Equation 3

$$\frac{1}{M_{Reuss}} = \sum_{i=1}^{N} \frac{f_i}{M_i},$$

where f_i and M_i are the volume fraction and modulus of the i´th component, respectively (Mavko et al., 1998).

The $V_{p,fluid}$ log is based on density, bulk modulus and V_p of the components of the fluid (here oil and brine). Here the effective bulk modulus of a homogeneous fluid K_{fluid} is calculated from Reuss average (Equation 3). The respective acoustic properties of each of the components of the fluid are based on empirical results summarised by Batzle and Wang (1992) and is controlled by the fluid builder parameters of Table 3 as a function of pressure and temperature.

The effective density of respectively solid and fluid are calculated as:

Equation 4

$$\rho_{eff} = \sum_{i=1}^{N} f_i \rho_i,$$

where f_i and ρ_i are the volume fraction and density of the i´th component, respectively.

Subject	Parameter	Value
Fluid builder	NaCl Sal	100000 ppm
	GOR	1100 scf/bbl
	Oil gravity	30 API
	Gas gravity	0.5 (specific)
	Gas index (brine; oil)	0; 0
Fluids	Brine (ρ; K)	1010 kg/m^3; 2.25 GPa
	Oil (ρ; K)	755 kg/m^3; 1.30 GPa
Mineralogy	Calcite (ρ; K; G)	2710 kg/m^3; 76.8 Gpa; 32 GPa
	Clay (ρ; K; G)	2580 kg/m^3; 32.0 GPa; 6.85 GPa

Table 3. Control parameters, used in the PetroTools constant manager. Here subdivided by subject.

Effective stress

The effective in situ stress in the formation at a specific depth is calculated from the effective overburden stress gradient and a reservoir pore pressure gradient.

The pore pressure gradient vary through the studied interval, due to differences in the composition of the reservoir fluid (here assumed to be an idealised mix of oil and brine). The general, initial reservoir pore pressure at South Arne is given as 6300 psi at -9200 ft TVDSS (personal communication with Amerada Hess A/S, 1999)

An initial pore pressure at top chalk of well SA-1 (calculated in Equation 5) and the pore pressure in the total interval (given in Equation 6 for the depth interval –9125; -9222 ft, TVDSS) are both based on the fluid gradients of Table 4 and the idealised fluid composition illustrated in Figure 1.

Equation 5.

$$P_{pore,tc} = 6300 psi - \left((9200 ft - 9125 ft) * (0.44 psi/ft * S_w + 0.33 psi/ft * (1 - S_w))\right) \Leftrightarrow$$
$$P_{pore,tc} = 6268 psi,$$

when S_w is 0.9 and $1\text{-}S_w\text{=}S_o$.

Equation 6.

$$P_{pore} = P_{p,datum} + (|z| - datum) * (S_w * 0.44 psi/ft + (1 - S_w) * 0.33 psi/ft) \Leftrightarrow$$
$$P_{pore} = 6268 psi + (|z| - 9125 ft) * 0.43 psi/ft,$$

where $P_{pore,datum}$ is 6268 psi, *datum* is -9125 ft, TVDSS, $S_w=0.9$, $1-S_w=S_o$, and z is numeric depth in ft, TVDSS. Note, in the three following intervals of Figure 1 ($P_{pore,datum}$, *datum*)-values are approximately (6309 psi, -9222 ft), (6366 psi, -9380 ft), and (6395 psi, -9460 ft).

The effective stress is calculated as external stress subtracted pore pressure. Since the sea depth is 197 ft and the overburden and water gradients is given in Table 4 (seawater and brine gradient is assumed identical), the effective stress can be calculated as:

Equation 7.

$$\sigma_{eff} = \left((z - 197\,ft) * 0.9\,psi/ft + 197\,ft * 0.44\,psi/ft\right) - P_{pore},$$

where P_{pore} is calculated from Equation 6.

Type of gradient	*Psi/ft*	*KPa/m*
Overburden gradient	0.90	20.25
Oil gradient	0.33	7.43
Brine/seawater gradient	0.44	9.90

Table 4. Gradients used to calculate effective stress in the formation.

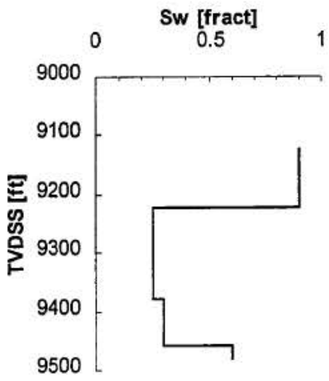

Figure 1. Idealised fluid composition of the studied well interval (S_o = 1 - S_w). Only used for estimating the effective in situ stress.

Acoustic and elastic properties

The acoustic and elastic properties are here studied with respect to depth, effective stress, pore fluid, and porosity.

Acoustic properties versus extrinsic parameters

Depth and stress. Plots of V_p, V_s, and V_p/V_s versus depth and effective in situ stress are given in Appendix 1 as Figure 2, Figure 3, and Figure 4.

As observed from Figure 2 and Figure 3, the compressional and shear velocities of the Tor Formation correlate with depth. The V_p and V_s of the Tor Formation data are almost constant with average values around 3585 m/s and 1990 m/s, respectively, and is characterised by a constant average V_p/V_s ratio at 1.80 (slightly decreasing with depth from a ratio above average to a ratio below average). The constant ratio of the Tor Formation data is in contrast to the large variation observed for the Ekofisk Formation data.

From Figure 4 it can be concluded, that there is no significant influence of the effective stress on the acoustic properties in the studied interval, since the acoustic properties are almost constant. The variation in the acoustic properties of the studied interval are – as described in the next section – coursed by influence of intrinsic parameters.

Acoustic and elastic properties versus intrinsic parameters

Pore fluid. Variations in V_p/V_s ratios can be induced by change in pore fluid. A comparison of the V_p/V_s ratio of Figure 3 with S_w of Figure 5 shows weak correlation between V_p/V_s ratios for the Ekofisk Formation (e.g. the drop in V_p/V_s ratio at depth 2805.5 m TVDSS corresponds to a drop in brine saturation). For the Tor Formation, the variations in fluid composition are insignificant in the acoustic data, since the variations in V_p/V_s can not be correlated with the variations in fluid composition. An average ratio of the Tor Formation data is approximately 1.80.

Figure 6, summarises the observations of both formations. A small increase in V_p/V_s is observed when the brine saturation is increased, but is only visible when large variations in fluid composition is observed (e.g. from S_w=30% to S_w=100%). The few Tor Formation data characterised by high brine saturation are all within the V_p/V_s-range characterising the low brine saturation Tor data. Therefore, a correlation between V_p/V_s and pore fluid is insignificant. This is in contrast to rock physics theory, when it is assumed that the acoustic properties of the solid phase is unchanged.

Porosity. In Figure 7, V_p/V_s versus porosity is illustrated. The Tor Formation data scatter less than Ekofisk Formation data, which have larger variation in both V_p/V_s ratio and porosity. No correlation between the two parameters is found for neither of the formations. Generally this can be explained by a strong correlation between V_p and V_s and porosity. This relationship can for the Tor Formation data be observed in Figure 8. Note, linear average trends are included. The increase in velocity due to decrease in porosity is lower than estimated by Raiga-Clemenceau *et al.* (1988) (Figure 10) and result in increasing differences between estimated and measured compressional velocities for the observed velocity interval. The velocity estimated by Wyllie *et al.* (1956) is underestimated (Figure 11). Note, that the input parameters of Wyllie´s equation (V_{fluid} and $V_{s,solid}$) is based on the simplified compositions of fluid and mineralogy (see Logs and control parameters). For the Ekofisk Formation data a velocity-porosity correlation is not observed (Figure 9). This seems unrealistic and put question to the quality of the Ekofisk data.

When V_p versus V_s is plotted the Tor Formation data correlates in contrast to the scatter of the Ekofisk Formation data (Figure 12).

Impedance (V_p *ρ, where ρ is bulk density) versus porosity also correlates for the Tor Formation data and a linear trend is included.

The elastic properties can be evaluated from the elastic moduli, which is defined on the principles of Hooke´s Law and from the assumption, that the rock behave as a linear, elastic material. Here, the elastic moduli are expressed from a dynamic viewpoint. Rock material responds to time harmonic external stress (or strain) induced by sound waves propagating through rock. This response is controlled by elastic stiffness and rock density, which means that the elastic moduli can be expressed from sound velocities and rock densities.

In Figure 14 and Figure 15, respectively bulk modulus and Poisson's ratio is plotted versus porosity. As expected, shows bulk modulus bulk modulus shows dependence of porosity, whereas Poisson's ratio does not. In Equation 8 and Equation 9 respectively bulk modulus (K) and Poisson´s ratio (ν) is defined from a dynamic viewpoint. Note, when two elastic moduli are known it is possible to calculate other elastic moduli.

Equation 8

$$K = \rho\left(Vp^2 - \tfrac{4}{3}Vs^2\right),$$

Equation 9

$$\nu = \frac{Vp^2 - 2Vs^2}{2(Vp^2 - Vs^2)},$$

where ρ is bulk density.

Fluid substitution

When comparing acoustic log data of different origin it is often useful to substitute from original fluid to e.g. brine to eliminate the fluid effect on acoustic properties.

The theory of fluid substitution based on Gassmann (1951)- Biot (1956) relations is resumed by Mavko *et al.* (1998), who is cited in the following:

Generally, when a rock is loaded under an increment of compression, such as from a passing seismic wave, an increment of pore pressure change is induced, which resists the compression and therefore stiffens the rock. The low-frequency Gassmann (1951)-Biot (1956) theory predicts the resulting increase in effective bulk modulus, K_{sat}, of the saturated rock through the following equation:

Equation 10

$$\frac{K_{sat}}{K_0 - K_{sat}} = \frac{K_{dry}}{K_0 - K_{dry}} + \frac{K_{fl}}{\varphi(K_0 - K_{fl})},$$

$$\mu_{sat} = \mu_{dry},$$

where

K_{dry} = *effective bulk modulus of dry rock*

K_{sat} = *effective bulk modulus of the rock with pore fluid*

K_0 = *bulk modulus of mineral material making up rock*

K_{fl} = *effective bulk modulus of pore fluid*

φ = *porosity*

μ_{dry} = *effective shear modulus of dry rock*

μ_{sat} = *effective shear modulus of rock with pore fluid*

Gassmann´s equation assumes a homogeneous meniral modulus and statistical isotrophy of the pore space but is free of assumptions about the pore geometry. Most importantly, it is valid only at sufficiently ***low frequencies*** *such that the induced pore pressures are equilibrated throughout the pore space (i.e., there is sufficient time for the pore fluid to flow and eliminate wave-induced pore pressure gradients). This limitation to low frequencies explains why Gassmann's relation works best for very low frequency in situ seismic data (<100 Hz) and may perform less well as frequencies increase toward sonic logging (≈10^4Hz) and laboratory ultrasonic measurements (≈10^6Hz).*

A substitution of the present fluid with brine is performed by the use of PetroTools, which is based on the theory just described (note, it is not correct just to replace K_{dry} in Equation 10 by $K_{new\ fluid}$). The theory above does not predict any change in shear modulus due to saturation, since there is no change in the net volume associated with shear deformations in an isotropic rock and therefore no compression of the pore fluid.

In PetroTools the bulk and shear modulus is calculated from V_p, V_s, and ρ (from a dynamic viewpoint), then the bulk modulus is transformed to represent the rock saturated with the new fluid, and then calculating the new velocities corresponding to the change in modulus. The bulk density that is used in the velocity-moduli relations are given by Equation 4 and is calculated from ρ_0, ρ_{fl}, and φ.

In Appendix 3 all figures represent the acoustic and the elastic responses to the rock saturated with the new, substituted fluid. The control parameters of the new fluid (100 % brine) are given in Table 3.

Figure 16 illustrates the new V_p and the Vs responses versus depth compared to the original response. As observed the modelled V_p is significantly higher than the original data in the hydrocarbon zone due to the increase in effective bulk modulus. The increase in fluid bulk modulus has stronger influence on the effective modulus than the increase in density. In contrast, the V_s theoretically decreases slightly because of an increase in density and a constant shear modulus. This leads to an increase in the V_p/V_s towards an average ratio of 1.95 as observed in Figure 17 and Figure 18.

The increase in V_p due to fluid substitution, results in a new velocity-porosity trend, which is given in Figure 19 (the original trend is given by a dotted line). Also in Figure 20 (V_p versus V_s) and Figure 21 (impedance versus porosity, the original trend is given by a dotted line) the effect of an increased V_p due to fluid substitution can be seen. Note,that the linear trends of Figure 19 and Figure 21 are almost parallel to the original trend, because the original S_w is almost constant.The dynamic moduli versus porosity presented in Figure 22 and Figure 23 also illustrates the effect of the changes in fluid toward higher moduli.

Discussion and conclusion

The variation in acoustic and elastic properties of the Tor Formation of well SA-1 has been studied with respect to the influence of effective stress, porosity, pore fluid.

Down through the depth interval of the Tor Formation, the effective stress increases from approximately 13.1 to 14.1 MPa. In this interval no increase in velocity due to increase in stress has be observed. When stress is constantly increased, the stress induced increase in velocity is expected to decrease. For the Tor Formation data, the observed independence between acoustic properties and effective stress therefore might be explained by the combination of a relatively high magnitude of the effective stress combined with a relatively small increase in stress.

Porosity influence on the acoustic and elastic properties of the studied chalk. The V_p/V_s ratio eliminates this influence of porosity and thus used for studying the influence of pore fluid. The acoustic properties of hydrocarbon saturated chalk and brine saturated chalk is hereby found to be insignificant. This might be explained by a variation in the acoustic properties of the solid phase or by a too small representation of high brine saturated data. An average ratio of the Tor Formation data is approximately 1.80 for the chalk saturated with original fluid and 1.95 for the chalk saturated with substituted fluid (S_w=100%).

Porosity is found to correlate with both compressional and shear wave velocity, impedance and bulk modulus. For the studied porosity interval (approximately 14%; 34%) linear average trends for the Tor Formation saturated with brine is found. The trends of V_p, V_s, and I are based on 798 data points which has undergone a Biot-Gassmann fluid substitution (Equation 11 to Equation 13).

Equation 11

$$V_p = -32\varphi + 4648,$$
$$R^2 = 0.26$$

Equation 12

$$V_s = -20\varphi + 2471,$$
$$R^2 = 0.19$$

Equation 13

$$I = V_p \rho = -0.14\varphi + 12.2,$$
$$R^2 = 0.55$$

where φ is given in %, velocity is given in m/s and I is given in 10^6*kg/m^3*m/s.

Parameters

DTCO	Delta-T (travel time) compressional wave.
DTSH	Delta-T (travel time) shear wave.
Eff_stress	Effective in situ stress.
GOR	Gas oil ratio.
I	Impedance calculated from density and compressional velocity.
MDRT	Measured depth from RT.
NaCl Sal	Salinity.
OWC	Oil water contact.
PHI_e	Interpreted porosity. Corrected for bore hole environment.
RHO_e	Interpreted bulk density. Bore hole environment corrected.
RT	Rotary.
ρ_{fl}	Density of pore fluid.
ρ_0	Density of the mineral that builds the rock.
Solid	The effective rock building mineral composition.
Solid	The effective rock building mineral composition.
SONIC	Delta-T (travel time) compressional wave. Sonic tool.
S_o	Oil saturation.
S_w	Brine saturation.
TVDRT	True vertical depth from RT.
TVDSS	True vertical depth from mean sea level (positive above sea level).
VCA	Volume calcite.
VSHmin	Volume shale, from gamma ray log.
V_p	Compressional velocity
V_s	Shear velocity

References

Armarada Hess A/S, 1998. Composite well log, SA-1, flank pilot.

Batzle, M., and Wang, Z., 1992. Seismic properties of pore fluids. *Geophysics*, 57, 1396-1408.

Biot, M. A.,1956.Theory of propagation of elastic waves in a fluid saturated porous solid. I. Low frequency range and II. Higher-frequency range. *J. Acoust. Soc. AM.*, 28, 168-191.

Gassmann, F., 1951. Elastic waves through a packing of spheres, *Geophysics*, 16, 673-685.

Japsen, P., 1998. Regional Velocity-Depth Anomalies, North Sea Chalk: A Record of Overpressure and Neogene Uplift and Erosion, *AAPG Bulletin*, 82, 2031-2074.

Mavko, G., Mukerji, T., Dvorkin, J., 1998. *The Rock Physics Handbook*, The Press Syndicate of the University of Cambridge, United Kingdom.

Raiga-Clemenceau, Martin, J., P., and Nicoletis, S., 1988. The concept of acoustic formation factor for more accurate porosity determination from sonic transit time data, *The Log Analyst*, 29, 54-60.

Wyllie, M. R. J., Gregory, A. R., and Gardner, L. W., 1956. Elastic wave velocities in hetrogeneous and pouros media, *Geophysics*, 21, 41-70.

Appendix 1

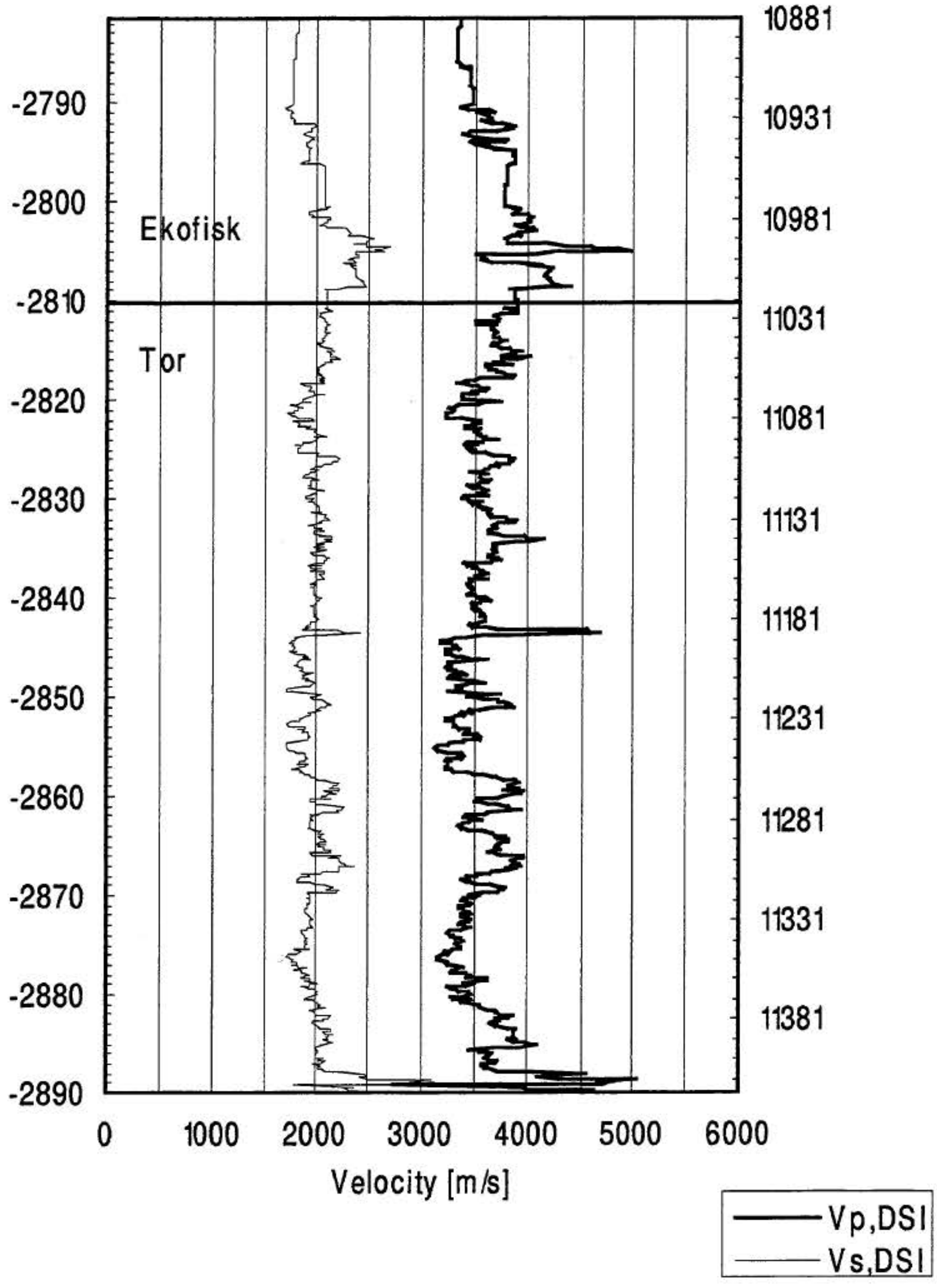

Figure 2. V_p and V_s versus depth for well SA-1.

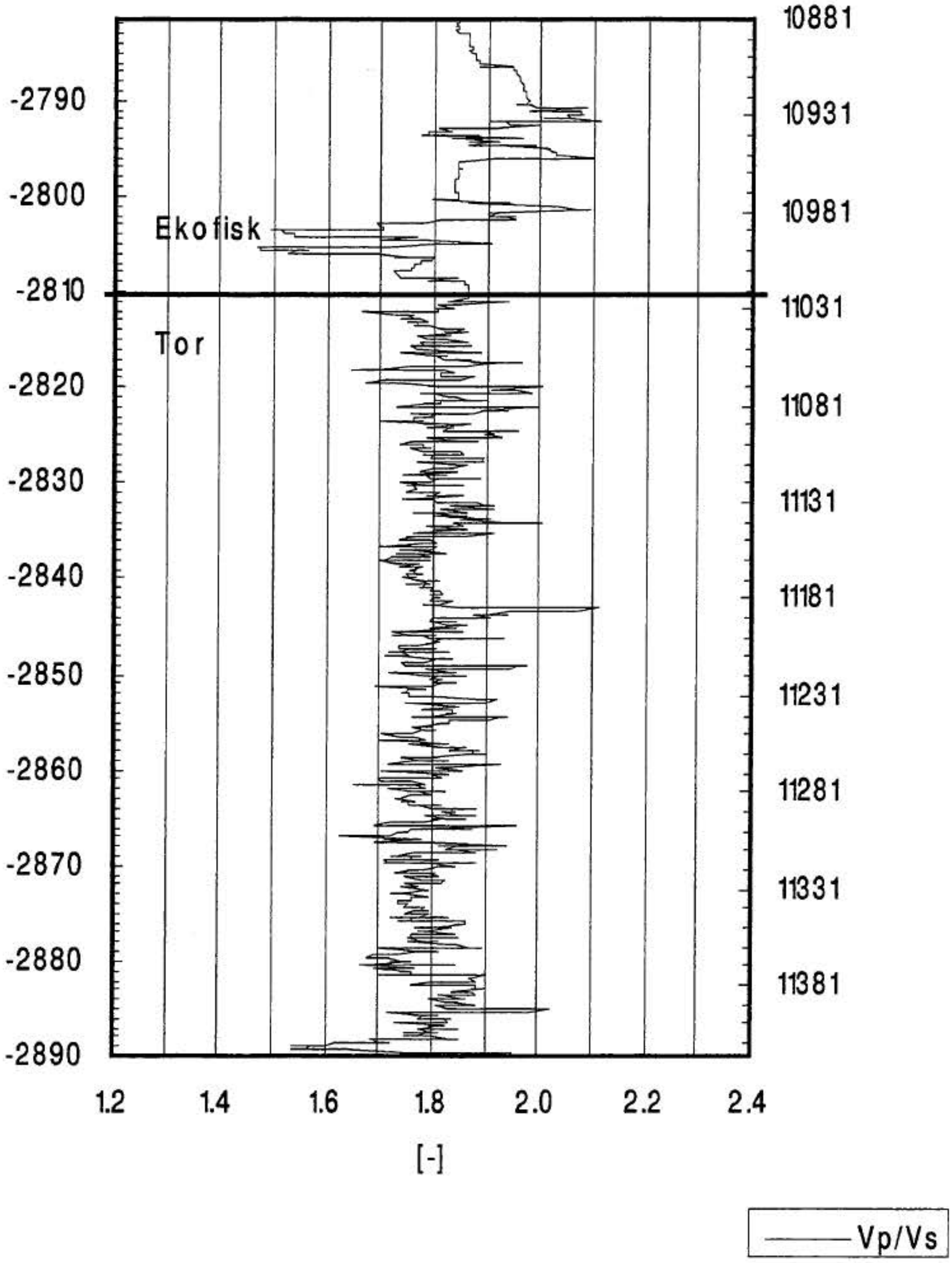

Figure 3. V_p / V_s versus depth for well SA-1.

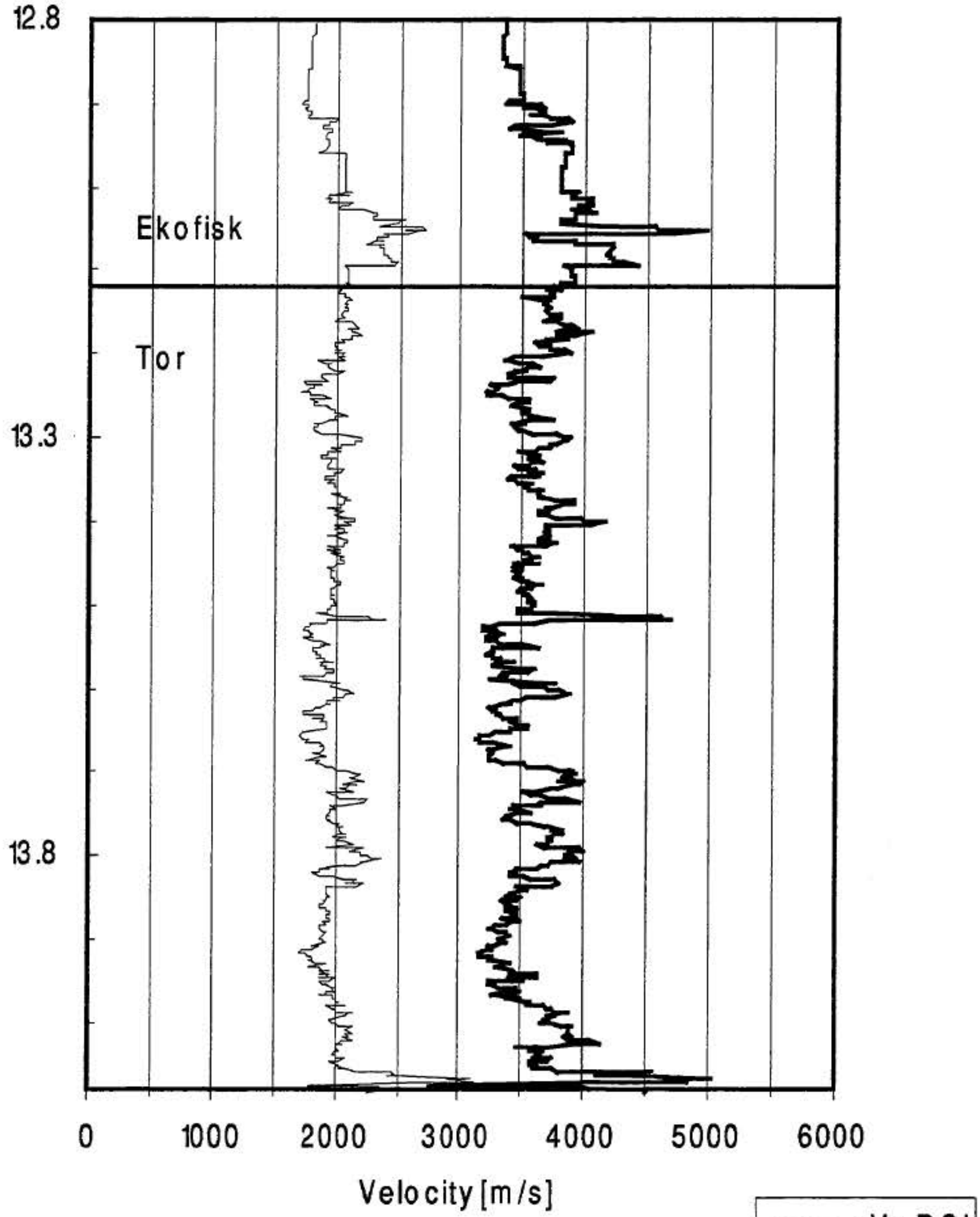

Figure 4. V_p and V_s versus effective in situ stress for well SA-1.

Appendix 2

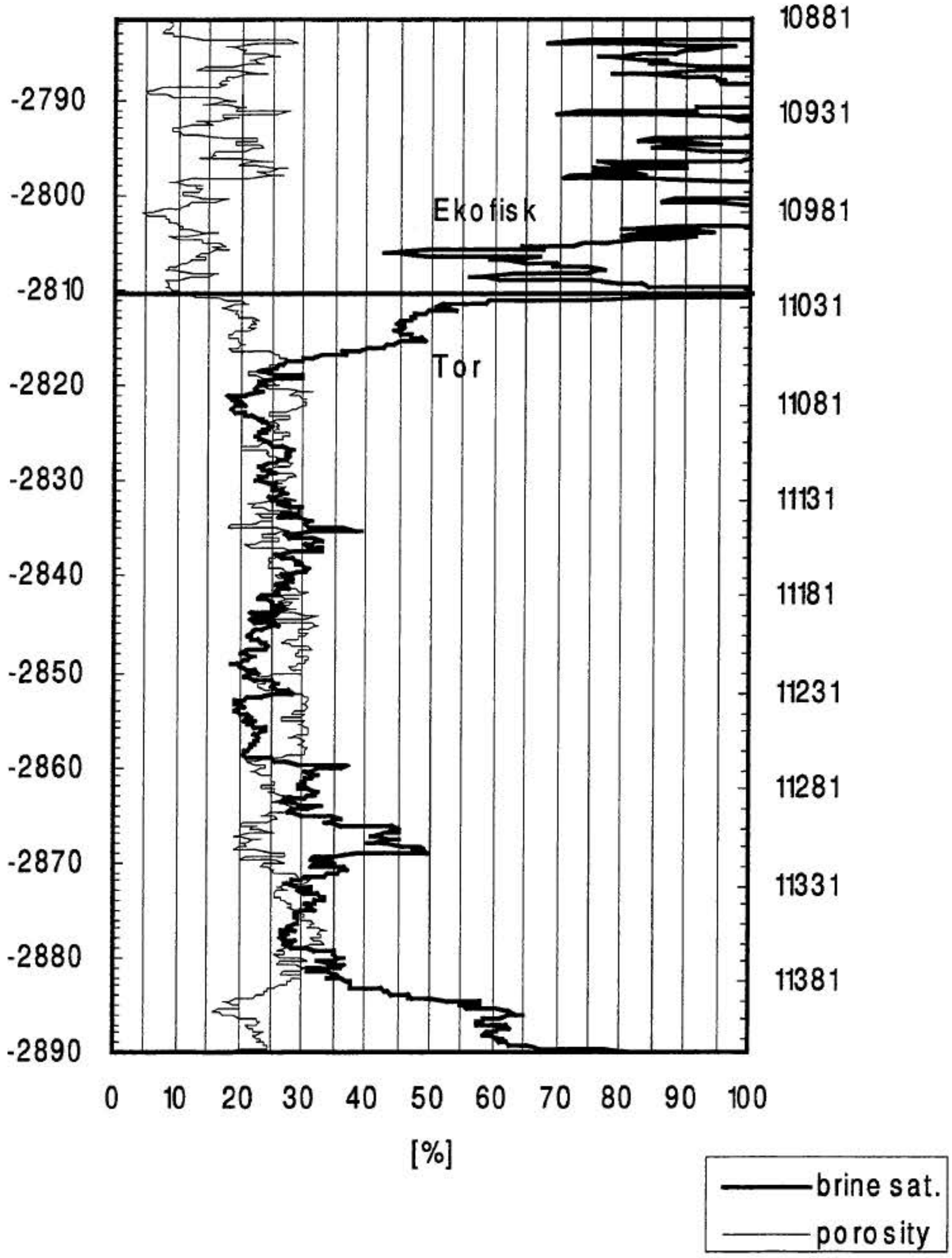

Figure 5. Depth versus brine saturation and porosity for well SA-1.

(Appendix 2 continued)

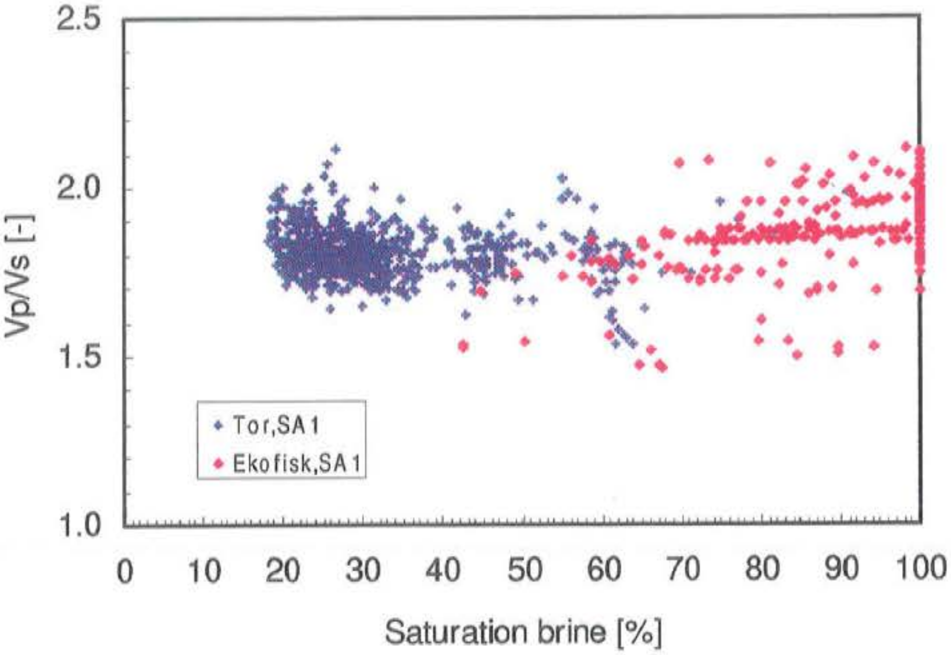

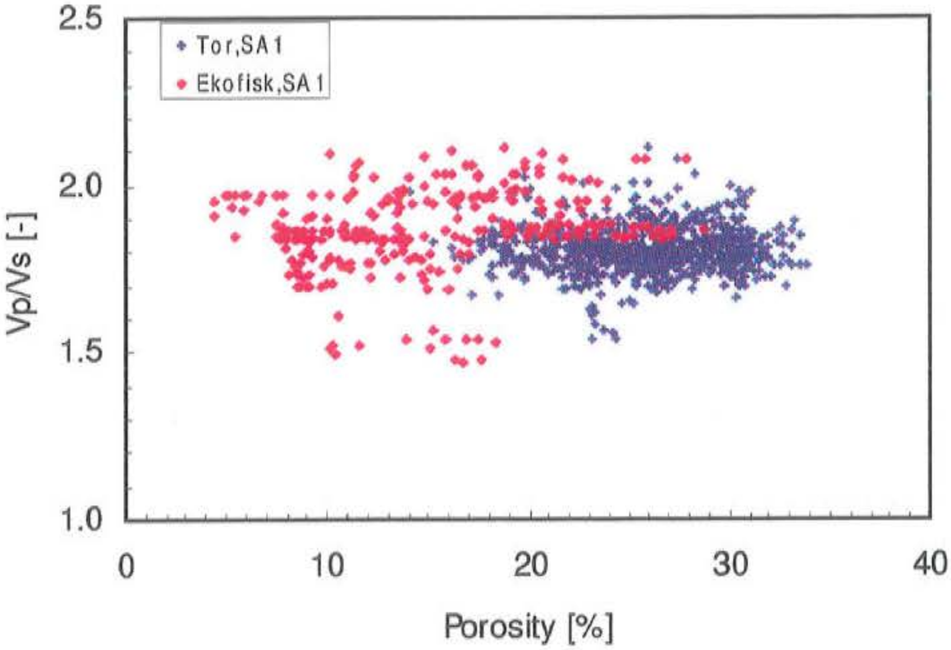

Figure 6 (top). V_p/V_s versus brine saturation for Tor and Ekofisk Formation, well SA-1 [no. of points in each figure: 798 (Tor), 294 (Ekofisk)].

Figure 7 (bottom). V_p/V_s versus porosity for Tor and Ekofisk Formation, well SA-1[no. of points in each figure: 798 (Tor), 294 (Ekofisk)].

(Appendix 2 continued)

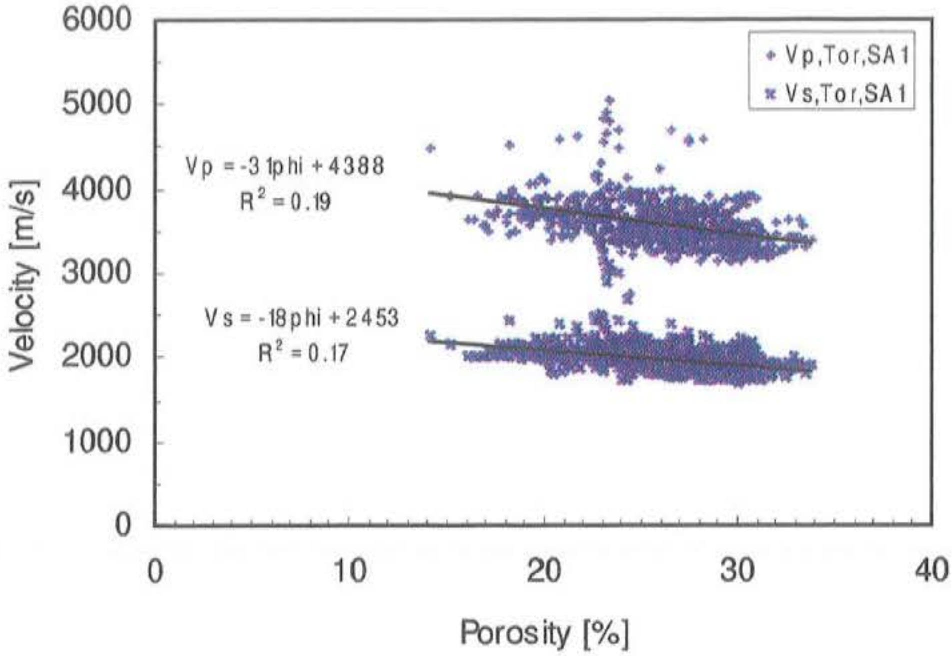

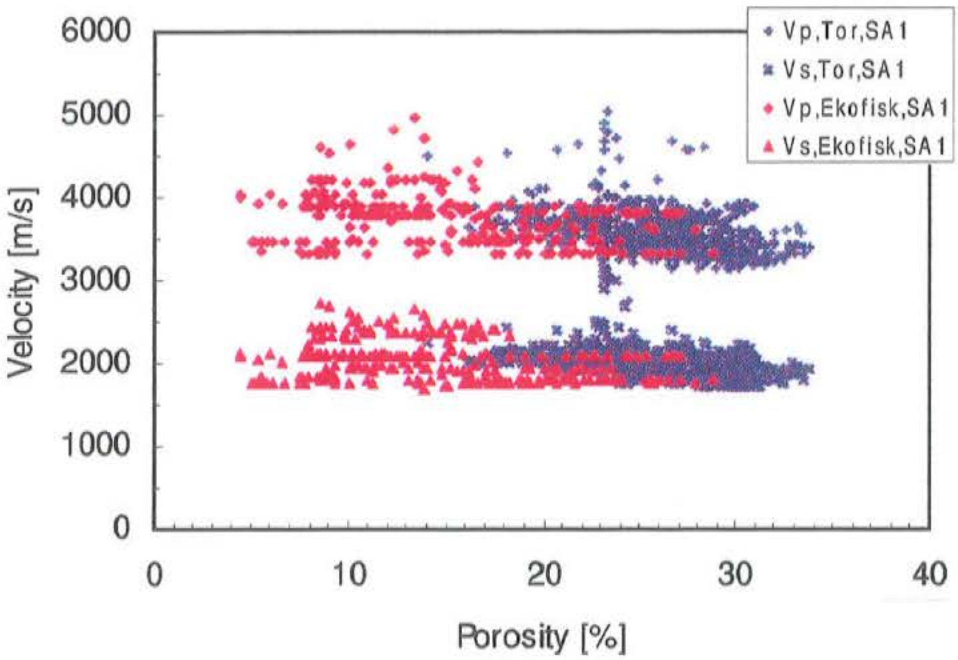

Figure 8 (top). V_p and V_s versus porosity for Tor Formation data, well SA-1[no. of points: 798 (Tor)].

Figure 9 (bottom). V_p and V_s versus porosity for Tor and Ekofisk Formation, well SA-1[no. of points: 798 (Tor), 294 (Ekofisk)].

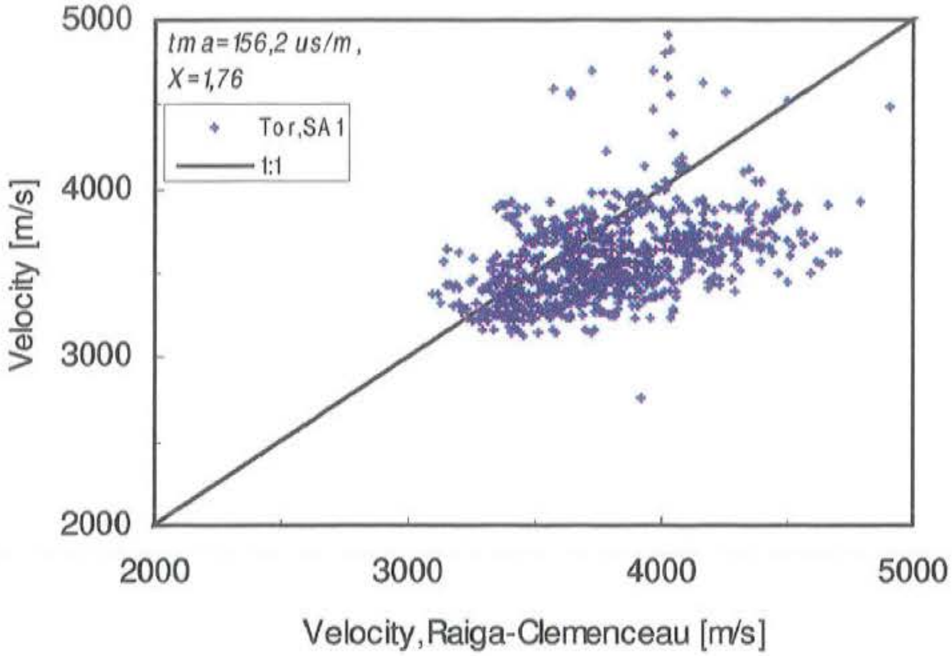

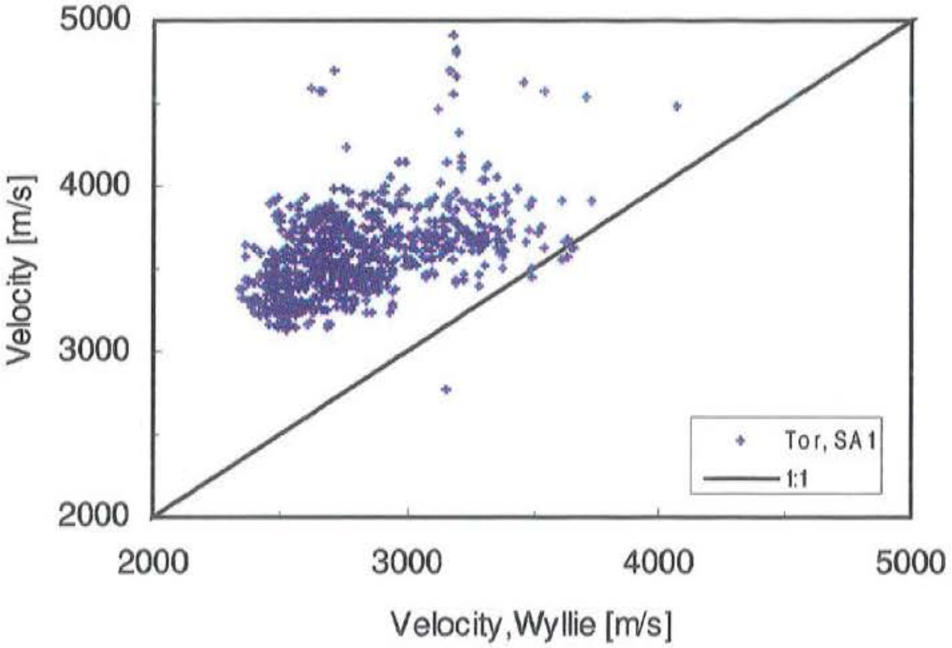

Figure 10 (top). Compressional velocity versus estimated velocity (Raiga-Clemenceau *et al.*, 1988) [no. of points 798].

Figure 11 (bottom). Compressional velocity versus estimated velocity (Wyllie *et al.*, 1956) [no. of points 798].

(Appendix 2 continued)

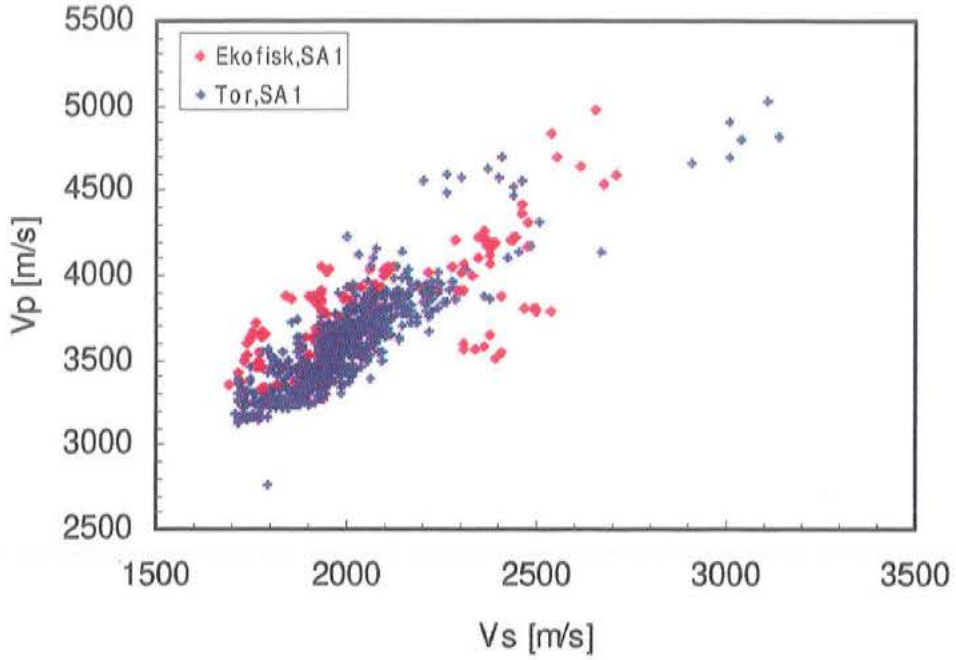

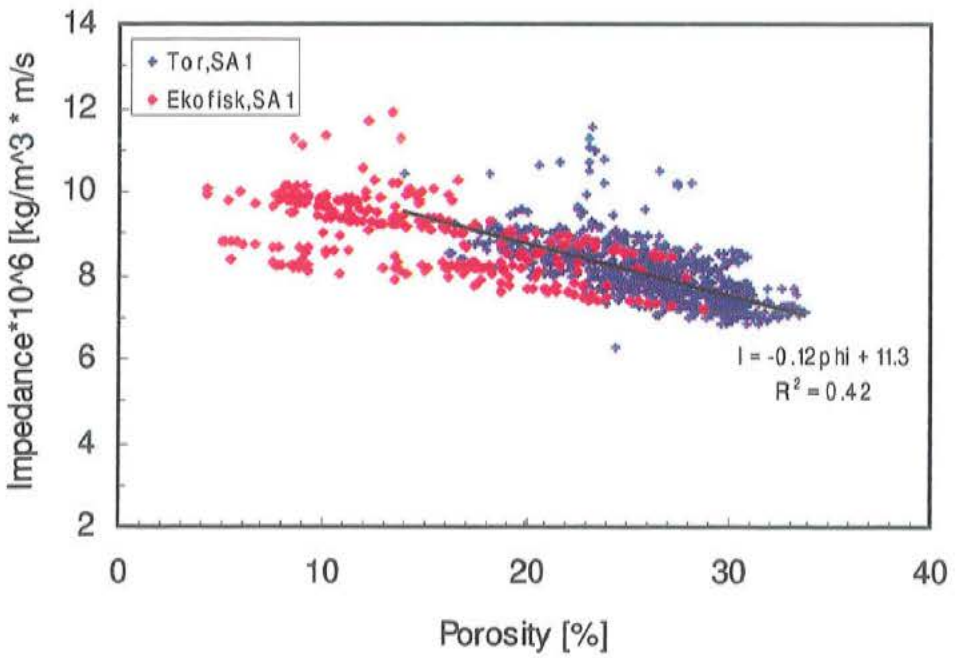

Figure 12(top). V_p versus V_s for Tor and Ekofisk Formations, well SA-1 [no. of points: 798 (Tor), 294 (Ekofisk)].

Figure 13(bottom). Impedance (V_p *ρ) versus porosity for Tor and Ekofisk Formations, well SA-1 [no. of points: 798 (Tor), 294 (Ekofisk)].

(Appendix 2 continued)

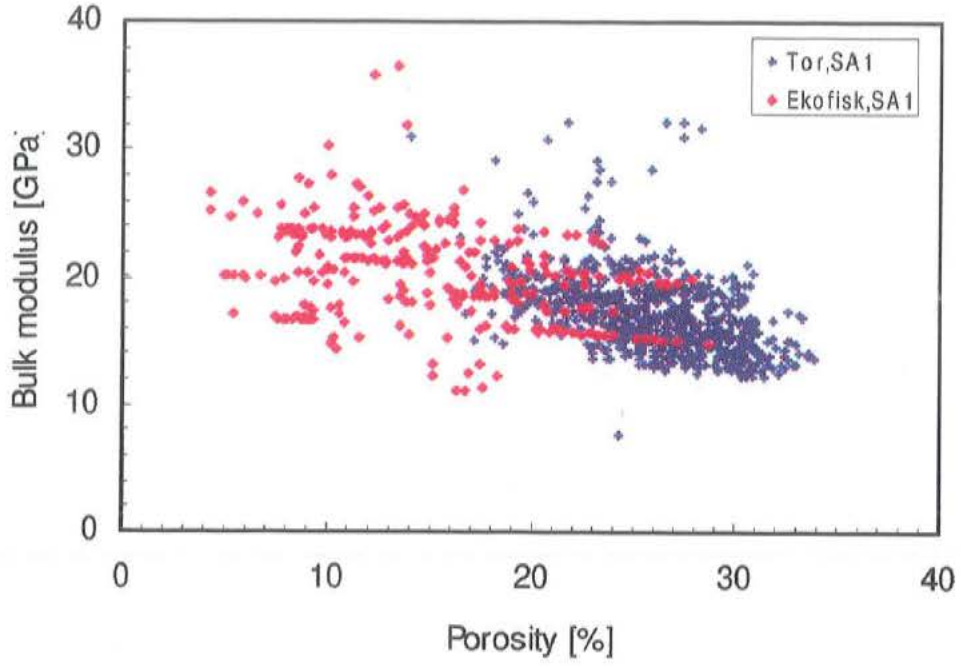

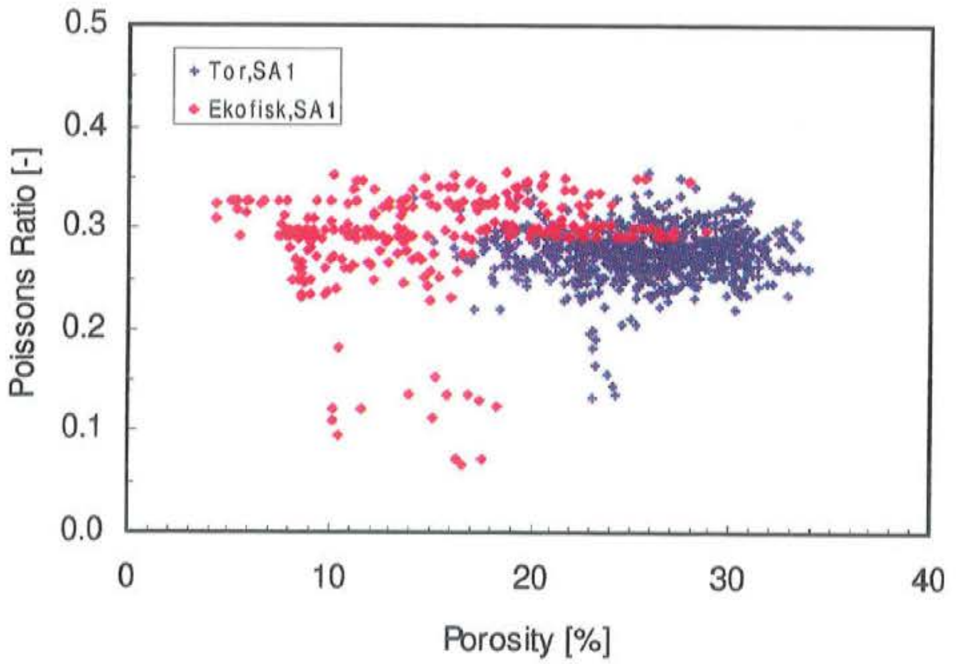

Figure 14(top). Bulk modulus versus porosity for Tor and Ekofisk Formation, well SA-1 [no. of points: 798 (Tor), 294 (Ekofisk)].

Figure 15 (bottom). Poisson´s ratio versus porosity for Tor and Ekofisk Formation, well SA-1 [no. of points figure: 798 (Tor), 294 (Ekofisk)].

Appendix 3

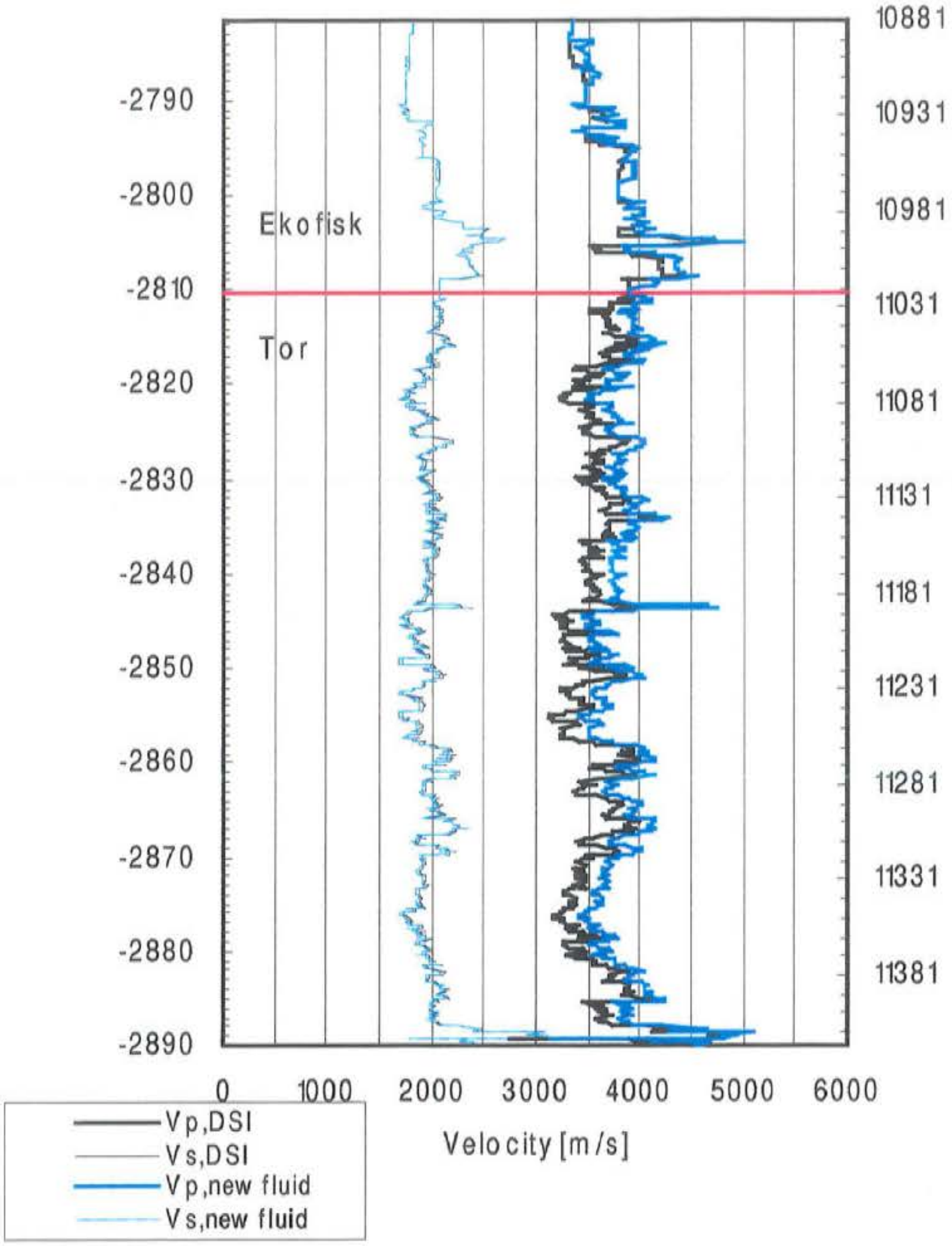

Figure 16. V_p and Vs versus depth for well SA-1. Acoustic response of rock saturated with substituted fluid is included (Sw=100%, light blue signature).

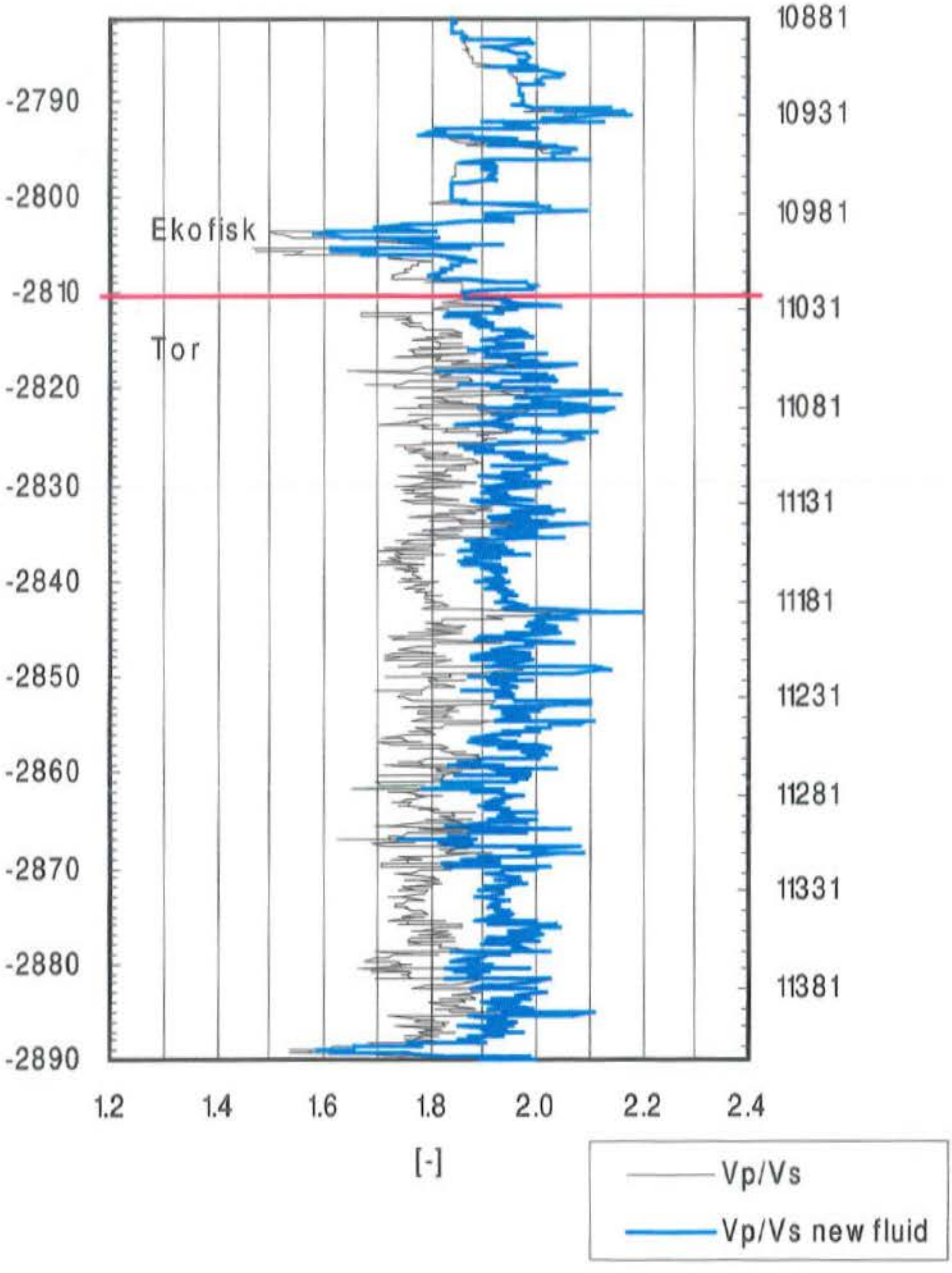

Figure 17. V_p/V_s versus depth for well SA-1. Acoustic response of rock saturated with substituted fluid included (Sw=100%, light blue signature).

(Appendix 3 continued)

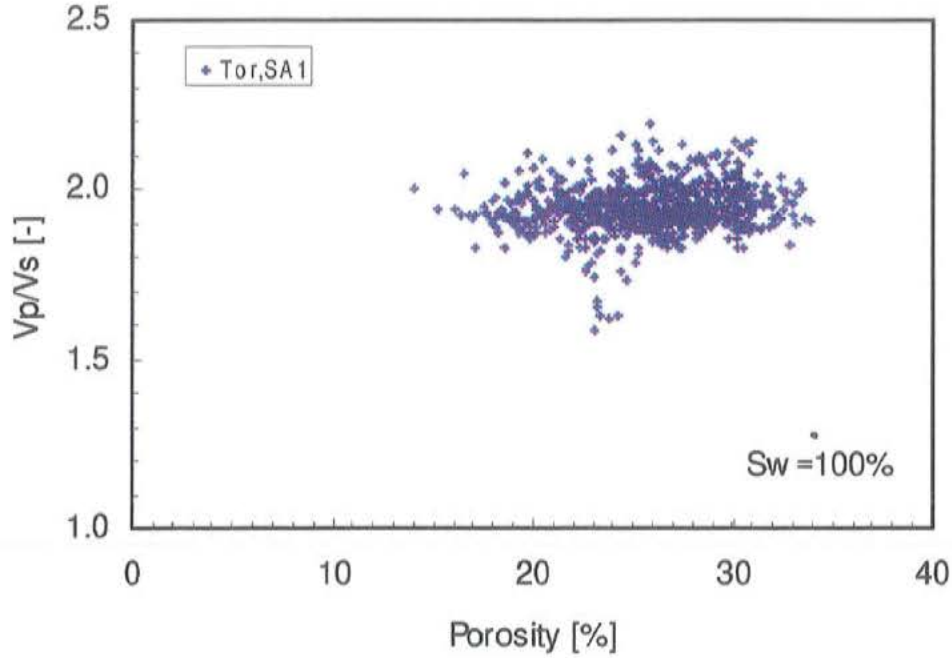

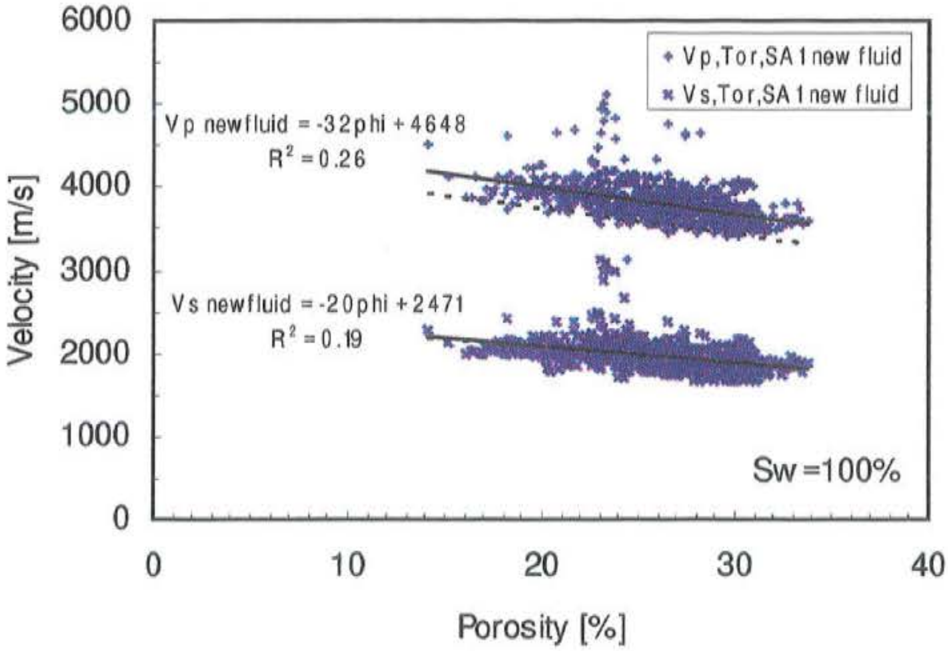

Figure 18(top). V_p/V_s versus porosity for Tor Formation, well SA-1. Acoustic response of the rock with substituted fluid (Sw=100%) [no. of points 798 (Tor)].

Figure 19 (bottom). V_p and V_s versus porosity for Tor Formation data, well SA-1. Acoustic response of the rock with substituted fluid (Sw=100%) [no. of points 798 (Tor)]. Linear trend of Figure 8 is included (dotted line signature).

(Appendix 3 continued)

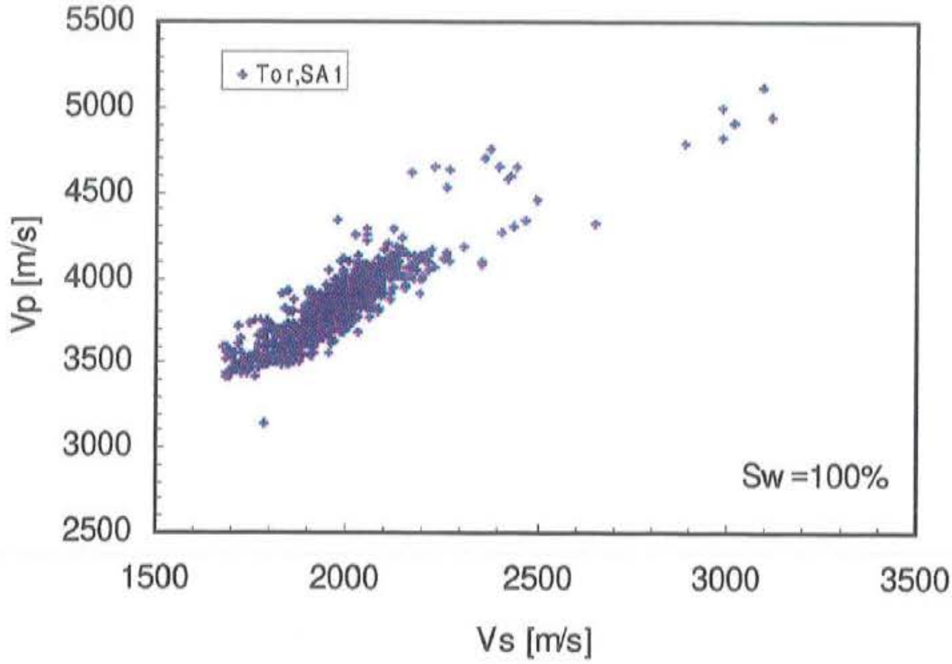

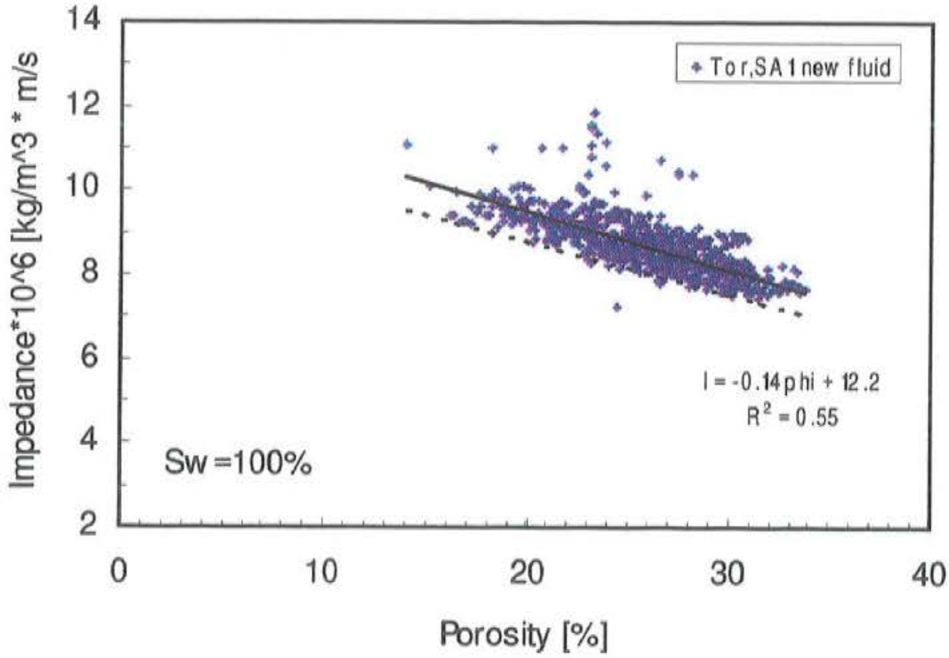

Figure 20 (top). V_p versus V_s for Tor Formation, well SA-1. Acoustic response of the rock with substituted fluid (Sw=100%) [no. of points 798 (Tor)].

Figure 21 (bottom). Impedance (V_p*ρ) versus porosity for Tor Formation data, well SA-1. Acoustic response of the rock with substituted fluid (Sw=100%) [no. of points 798 (Tor)]. Linear trend of Figure 8 is included (dotted line signature).